



Modeling magnetically levitated superconducting ellipsoids, cylinders, and cuboids for quantum magnetomechanics








Downloaded from: <https://research.chalmers.se>, 2024-11-05 23:21 UTC

Citation for the original published paper (version of record):

Bort-Soldevila, N., Cunill-Subiranas, J., Del-Valle, N. et al (2024). Modeling magnetically levitated superconducting ellipsoids, cylinders, and cuboids for quantum magnetomechanics. *Physical Review Research*, 6(4).
<http://dx.doi.org/10.1103/PhysRevResearch.6.043046>

N.B. When citing this work, cite the original published paper.

Modeling magnetically levitated superconducting ellipsoids, cylinders, and cuboids for quantum magnetomechanics

Natanael Bort-Soldevila ^{1,*}, Jaume Cunill-Subiranas ^{1,*}, Nuria Del-Valle ¹, Witlef Wiczorek ², Gerard Higgins ^{2,3},
Michael Trupke ^{3,4} and Carles Navau ^{1,†}

¹*Departament de Física, Universitat Autònoma de Barcelona, 08193 Bellaterra, Barcelona, Spain*

²*Department of Microtechnology and Nanoscience (MC2), Chalmers University of Technology, SE-412 96 Gothenburg, Sweden*

³*Institute for Quantum Optics and Quantum Information (IQOQI), Austrian Academy of Sciences, A-1090 Vienna, Austria*

⁴*Vienna Center for Quantum Science and Technology, Department of Physics, University of Vienna, A-1090 Vienna, Austria*



(Received 23 April 2024; accepted 30 September 2024; published 17 October 2024)

We theoretically investigate the properties of magnetically levitated superconducting elements confined in anti-Helmholtz traps, for application in magnetomechanical experiments. We study both the translational modes and the librational mode. The librational mode gives an additional degree of freedom that levitated spheres do not have access to. We compare levitated particles of different shapes: ellipsoids (with analytical and numerical treatment), cylinders, and rectangular cuboids (numerical treatment). We find that the stable orientations of the particles depend on their aspect ratios.

DOI: [10.1103/PhysRevResearch.6.043046](https://doi.org/10.1103/PhysRevResearch.6.043046)

I. INTRODUCTION

When an external uniform magnetic field \mathbf{H}_a is applied over a magnetic material with the shape of an ellipsoid, it magnetizes with a uniform magnetization \mathbf{M} [1]. If the magnetic material is linear, $\mathbf{B} = \mu\mathbf{H}$ inside the ellipsoid (μ is the constant permeability), and the magnetization is related to the internal field through the susceptibility constant χ as $\mathbf{M} = \chi\mathbf{H}$. Thus, $\chi = (\mu/\mu_0) - 1$, where μ_0 is the vacuum permeability.

When $\mu \rightarrow 0$ ($\chi \rightarrow -1$) the material behaves as a perfect diamagnet ($\mathbf{B} = 0$ inside). A superconductor can be modeled as a perfect diamagnet, although there are extra properties, i.e., flux quantization, that are not captured by just $\chi \rightarrow -1$. On the other limit, when $\mu \rightarrow \infty$ ($\chi \rightarrow \infty$) we would be considering a perfectly soft ferromagnet ($\mathbf{H} = 0$ inside).

The demagnetizing factors are commonly used in magnetic experiments. Indeed, the experimentalist controls the applied field, while the intrinsic properties one usually wants to measure (i.e., the susceptibility) depend on the internal field. Both are related through the demagnetizing factors.

We focus our study on levitation systems in the context of quantum magnetomechanics. Indeed, the levitation of small diamagnetic microparticles in specially designed magnetic traps has been proposed as the experimental platform to perform ground-state cooling of the center-of-mass degrees

of freedom of the superconductor [2–4]. Different magnetic traps have been proposed, such as surface superconductors [5–7], quadrupolar magnets [8], chip-based multi-winding planar coils [4], 3D arranged coils [3], or anti-Helmholtz coils (AHCs) [2], to cite some. Stable levitation of lead microspheres ($\simeq 50 \mu\text{m}$ in diameter, 700 ng of mass) in anti-Helmholtz traps has been recently demonstrated [4,9]. Using a similar system (with elliptical coils to break the xy -axis symmetry) the center-of-mass motion of levitated lead-tin spheres (now of $\simeq 100 \mu\text{m}$ in diameter) have been feedback controlled after coupling with a superconducting quantum interference device achieving quality factors up to 2.6×10^7 [10].

As for the applied field, we shall consider AHCs generating the applied fields. In these levitation experiments, the applied field is not uniform and the use of demagnetizing factors should be carefully considered. At the equilibrium position, the applied field is quadrupolar with a value of zero at the center. The assumption of a uniform applied field does not apply. However, we will see how to take advantage of the demagnetizing factors to account for the restoring force and obtain useful expressions for the trapping frequency.

As for the levitated particle, not only the size, but its shape can play an important role, since the demagnetizing fields can change drastically the total field it experiences. Although the spherical shape is the most used in magnetomechanics levitation experiments [11], finding a perfect sphere is complicated and studying how the shape affects the levitation is important. The nonsphericity lifts some of the symmetries and some vibrational modes become nondegenerate. Moreover, nonspherical particles exhibit torques in the nonuniform magnetic field which lead to librational modes (rotational oscillations) as additional degrees of freedom [12]. Ellipsoids represent a good approximation for many other shapes ranging from long cylinders to disks (and including the sphere). Although the levitation of superconducting rings (including flux

*These authors contributed equally to this work.

†Contact author: carles.navau@uab.cat

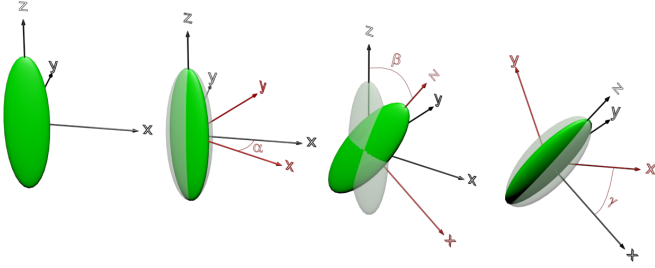


FIG. 1. Sketch of a general rotation of an ellipsoid. The axes after rotating the ellipsoid are red, and the ellipsoid once rotated is intense green. When $a = b$, the α angle can be skipped and the γ angle is irrelevant (since x and y are identical). Thus, when $a = b$, only β is a relevant rotation angle.

quantization) has been considered [11,13], there is a lack of work devoted to studying the superconductor's shape influence.

In this work, we aim to conduct an investigation of the levitation characteristics of magnetic particles in a quadrupolar (anti-Helmholtz) magnetic trap. We mainly focus on superconducting ellipsoids, but some comparison with cylinders and rectangular cuboids is also presented. For the ellipsoids, we derive analytic expressions for the translational trapping frequencies as a function of the principal axis lengths. For the librational frequencies, as well as for the comparison with cylinders and rectangular cuboids, we use finite-element simulations.

The paper is structured as follows. In Sec. II we derive the expressions for the magnetization of a generic ellipsoidal linear magnetic material in the presence of a uniform applied field. We find the external susceptibility matrix that relates the magnetization of the ellipsoid with the external applied field. In Sec. III, we consider a quadrupolar field and find how the forces and torques over the levitated ellipsoid near its center can be found. We evaluate the translational and librational torques for this trap. In Secs. III C and III D, numerical results comparing translational and librational frequencies, respectively, of the trap for levitated superconducting ellipsoids,

cylinders, and rectangular cuboids are presented. We finish with conclusions in Sec. IV.

II. THE EXTERNAL SUSCEPTIBILITY FOR ELLIPSOIDS

We consider a linear magnetic material with susceptibility χ (an ideal superconductor would be $\chi = -1$) and with the shape of an ellipsoid with principal semiaxes a , b , and c . The induction field \mathbf{B} inside the ellipsoid is related to the magnetization \mathbf{M} , the magnetic field \mathbf{H} , the applied field \mathbf{H}_a (uniform, in this section), and the demagnetizing field \mathbf{H}_d , through

$$\mathbf{B} = \mu_0(\mathbf{M} + \mathbf{H}) = \mu_0(\mathbf{M} + \mathbf{H}_a + \mathbf{H}_d). \quad (1)$$

The magnetization of the ellipsoid is related to the demagnetizing field through the diagonal demagnetizing factor matrix \mathbb{N} when both \mathbf{M} and \mathbf{H}_d components are expressed as projections along the principal axes (\hat{a} , \hat{b} , and \hat{c}) of the ellipsoid. In this case, one has $\mathbf{H}'_d = -\mathbb{N}\mathbf{M}'$ where the primes ($'$) indicate projections along principal axes and

$$\mathbb{N} = \begin{pmatrix} N_a & 0 & 0 \\ 0 & N_b & 0 \\ 0 & 0 & N_c \end{pmatrix}. \quad (2)$$

The demagnetizing factors N_a , N_b , and N_c satisfy $N_a + N_b + N_c = 1$. Using Eq. (1),

$$\mathbf{M}' = \chi(\mathbb{1} + \chi\mathbb{N})^{-1}\mathbf{H}'_a. \quad (3)$$

We describe the orientation of the ellipsoid using the Euler angles zyz representation of rotation [14] defined as follows (see Fig. 1): (i) Initially the ellipsoid's principal axis coincides with the Cartesian axis, $\hat{a} = \hat{x}$, $\hat{b} = \hat{y}$, and $\hat{c} = \hat{z}$; (ii) first, rotate the ellipsoid an angle α with respect to the z axis; (iii) second, rotate the (already rotated) ellipsoid an angle β with respect to the rotated y axis; (iv) finally, rotate the (already rotated) ellipsoid an angle γ with respect to the rotated z axis.

Any rotation within this representation can be described by (α, β, γ) . The rotation matrix \mathbb{Q} is

$$\mathbb{Q} = \begin{pmatrix} \cos \alpha \cos \beta \cos \gamma - \sin \alpha \sin \gamma & -\cos \gamma \sin \alpha - \cos \alpha \cos \beta \sin \gamma & \cos \alpha \sin \beta \\ \cos \beta \cos \gamma \sin \alpha + \cos \alpha \sin \gamma & \cos \alpha \cos \gamma - \cos \beta \sin \alpha \sin \gamma & \sin \alpha \sin \beta \\ -\cos \gamma \sin \beta & \sin \beta \sin \gamma & \cos \beta \end{pmatrix}. \quad (4)$$

We use this \mathbb{Q} matrix to change the coordinates of the vectors. Actually, we have $\mathbf{H}'_a = \mathbb{Q}\mathbf{H}_a$ or $\mathbf{H}_a = \mathbb{Q}^T\mathbf{H}'_a$, where T indicates the transposed matrix. From Eq. (3) we can write the magnetization vector, expressed in Cartesian coordinates as a function of the *applied* field, also expressed in Cartesian coordinates:

$$\mathbf{M} = \mathbb{S}\mathbf{H}_a, \quad (5)$$

where we have defined the *external susceptibility matrix* \mathbb{S} as

$$\mathbb{S} = \chi\mathbb{Q}^T(\mathbb{1} + \chi\mathbb{N})^{-1}\mathbb{Q}. \quad (6)$$

The importance of Eq. (5) relies on that it gives the magnetization of an arbitrarily rotated linear, homogeneous,

isotropic, and magnetic ellipsoid as a consequence of a uniform applied field, directly as a function of the applied field (not the internal field \mathbf{H}). The obtained matrix \mathbb{S} is general and can be applied to any ellipsoid as long as the applied field is considered uniform through the ellipsoid. The explicit general expression is cumbersome although straightforward from Eqs. (2), (4), and (6).

Spheroid, $a = b$

As a particular case of the general treatment done above, we consider here that the ellipsoid has two identical principal axes, $a = b$. Then, $N_a = N_b \equiv N_{ab}$. Considering the applied

field along the z direction, any rotation is described only by β . That is, we are rotating the spheroid about the y axis at an

angle β . In this case, the external susceptibility matrix reduces to

$$\mathbb{S} = \begin{pmatrix} \frac{\chi[(N_{ab}+N_c)\chi - (N_{ab}-N_c)\cos(2\beta)\chi + 2]}{2(N_{ab}\chi + 1)(N_c\chi + 1)} & 0 & \frac{(N_c - N_{ab})\chi^2 \cos \beta \sin \beta}{(N_{ab}\chi + 1)(N_c\chi + 1)} \\ 0 & \frac{\chi}{N_{ab}\chi + 1} & 0 \\ \frac{(N_c - N_{ab})\chi^2 \cos \beta \sin \beta}{(N_{ab}\chi + 1)(N_c\chi + 1)} & 0 & \frac{\chi[(N_{ab}+N_c)\chi + (N_{ab}-N_c)\cos(2\beta)\chi + 2]}{2(N_{ab}\chi + 1)(N_c\chi + 1)} \end{pmatrix}. \quad (7)$$

Importantly, for the spheroid, the demagnetizing factors of \mathbb{N} have been analytically found [15–17] as

$$N_c = \begin{cases} \frac{1}{1 - (\frac{c}{a})^2} \left(1 - \frac{\frac{c}{a}}{\sqrt{1 - (\frac{c}{a})^2}} \arccos \frac{c}{a} \right), & \text{if } c < a, \\ \frac{1}{(\frac{c}{a})^2 - 1} \left[\frac{\frac{c}{a}}{\sqrt{1 - (\frac{c}{a})^2}} \ln \left(\frac{c}{a} + \sqrt{(\frac{c}{a})^2 - 1} \right) - 1 \right], & \text{if } c > a, \end{cases} \quad (8)$$

$$N_{ab} = \frac{1}{2}(1 - N_c). \quad (9)$$

In Figs. 2 and 3 we plot the values of different components of the \mathbb{S} matrix as a function of c/a for several values of β and χ . When $\beta = 0$ and when $\beta = \pi/2$ one obtains, respectively,

$$\mathbb{S}(\beta = 0) = \begin{pmatrix} \frac{\chi}{N_{ab}\chi + 1} & 0 & 0 \\ 0 & \frac{\chi}{N_{ab}\chi + 1} & 0 \\ 0 & 0 & \frac{\chi}{N_c\chi + 1} \end{pmatrix}, \quad (10)$$

$$\mathbb{S}(\beta = \pi/2) = \begin{pmatrix} \frac{\chi}{N_c\chi + 1} & 0 & 0 \\ 0 & \frac{\chi}{N_{ab}\chi + 1} & 0 \\ 0 & 0 & \frac{\chi}{N_{ab}\chi + 1} \end{pmatrix}. \quad (11)$$

For spheres, $N_c = N_{ab} = 1/3$, the rotation matrix is the identity matrix, and the external susceptibility tensor becomes

$$\mathbb{S} = \frac{3\chi}{3 + \chi} \mathbb{1}. \quad (12)$$

For the ideal superconducting sphere ($\chi = -1$), we have $\mathbb{S} = -(3/2)\mathbb{1}$.

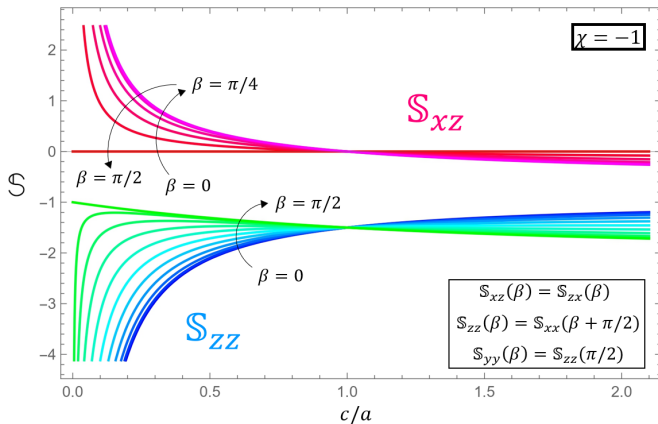


FIG. 2. S_{zz} (blue-green) and S_{xz} (red-purple) matrix elements of a spheroid, as a function of c/a for different values of β from 0 to $\pi/2$ in intervals of $\pi/20$ (following the arrows). In this figure, $\chi = -1$. Note that the rest of the matrix is given by $S_{zx}(\beta) = S_{xz}(\beta)$, $S_{zz}(\beta) = S_{xx}(\beta + \pi/2)$, $S_{yy}(\beta) = S_{xx}(0) = S_{zz}(\pi/2)$, and $S_{xy} = S_{yx} = S_{yz} = S_{zy} = 0$.

III. FORCES AND TORQUES OVER THE ELLIPSOID IN A QUADROPOLAR EXTERNAL FIELD

A. Anti-Helmholtz coil field

One of the common traps for quantum magnetomechanics experiments is the AHC trap. It consists of two coaxial coils of radius R separated by a distance R . A current I circulates through the coils in the opposite direction. The origin of coordinates is located on the coaxial axis of the coils, at the equidistant point between all the points of both coils. The field created by the AHC at positions $\mathbf{r} = (x, y, z)$ close to the origin ($|\mathbf{r}| \ll R$) is a quadrupolar field that can be written as

$$\mathbf{H}_a = \frac{H_0}{R}(-x\hat{\mathbf{x}} - y\hat{\mathbf{y}} + 2z\hat{\mathbf{z}}), \quad (13)$$

where $H_0 \equiv \frac{24I}{25\sqrt{5}R}$.

We consider a, b , and c small enough with respect to R so that in all situations, all the points of the ellipsoid will be on the region where Eq. (13) holds.

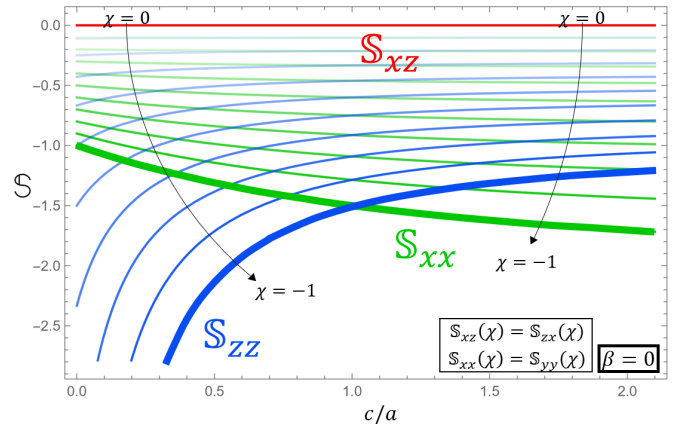


FIG. 3. S_{xx} (green), S_{zz} (blue), and S_{xz} (red) matrix elements of a spheroid, as a function of c/a for different values of χ , from 0 to -1 in intervals of -0.1 (following the arrows). The thickest lines correspond to curves with $\chi = -1$. In this figure, $\beta = 0$. Note that the rest of the matrix is given by $S_{zx}(\chi) = S_{xz}(\chi)$, $S_{xx}(\chi) = S_{yy}(\chi)$, and $S_{xy} = S_{yx} = S_{yz} = S_{zy} = 0$.

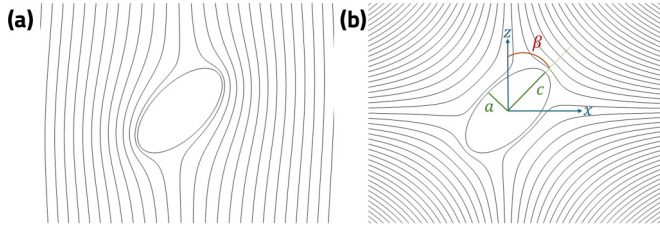


FIG. 4. Magnetic field lines interacting with a diamagnetic ellipsoid, (a) for a uniform external magnetic field and (b) for an external quadrupolar magnetic field.

To simplify the treatment we shall consider, unless explicitly indicated, that we have a perfectly diamagnetic ($\chi = -1$) ellipsoid with $a = b$ (a spheroid), near the center of the trap. In Fig. 4 we show an example of field lines for a uniform applied field and an AHC field.

B. Forces after translations

The stable position for translation of a levitated spheroid is when its center coincides with the center of the AHC, where the applied field is zero (we neglect gravity). Any translation of the ellipsoid from this position results in a restoring force that tends to push the ellipsoid to the center again.

In general, the magnetization inside the ellipsoid is not uniform. Since we are considering a region where the applied field is linear, if the center of the ellipsoid is moved to a point \mathbf{r}_0 , we have

$$\mathbf{H}_a(\mathbf{r}) = \mathbf{H}_a(\mathbf{r}_0) + \mathbf{H}_a(\mathbf{r}'), \quad (14)$$

where $\mathbf{r}' = \mathbf{r} - \mathbf{r}_0$ points to an ellipsoid's point *as if it were located at the origin*.

As we have assumed linear materials, the magnetization of the spheroid will be the sum of the magnetization induced by these two fields. The currents induced by the second term will have a complicated distribution but, because of the symmetry, the forces they receive sum up to zero when integrated all over the spheroid's surface.

Thus, *as far as the force evaluation is concerned*, we can consider only the currents induced because of the field given by the first term of the right-hand side of Eq. (14). That is, the force exerted over the ellipsoid with its center at \mathbf{r}_0 can then be written, using Eq. (5), as

$$\mathbf{F} = \mu_0 V (\mathbf{S} \mathbf{H}_a \cdot \nabla) \mathbf{H}_a \Big|_{\mathbf{r}=\mathbf{r}_0}, \quad (15)$$

where V is the volume of the spheroid and the applied field and its derivatives should be evaluated at \mathbf{r}_0 , the “displaced” center of the spheroid (see Appendix A for a detailed demonstration).

The trapping frequencies are then evaluated from the variations of the force components with respect to the coordinates ($x_l = x, y, \text{ or } z$):

$$\omega_{kl} = \sqrt{\frac{1}{m} \left(- \frac{\partial F_k}{\partial x_l} \Big|_{x_l \rightarrow 0} \right)}, \quad (16)$$

where m is the mass of the ellipsoid. Using Eqs. (13) and (15) one gets

$$\omega_{xx} = \omega_0 \sqrt{-\mathcal{S}_{xx}}, \quad (17)$$

$$\omega_{yy} = \omega_0 \sqrt{-\mathcal{S}_{yy}}, \quad (18)$$

$$\omega_{zz} = 2\omega_0 \sqrt{-\mathcal{S}_{zz}}, \quad (19)$$

where ω_0 is defined as

$$\omega_0 = \frac{H_0}{R} \sqrt{\frac{\mu_0}{\varrho}}, \quad (20)$$

ϱ being the mass density of the ellipsoid. When $\beta = 0$ or $\beta = \pi/2$, $\omega_{kl} = 0$ for all $k \neq l$. For an ideal superconducting sphere, Eqs. (17)–(19) reduce to $\omega_{xx} = \omega_{yy} = (1/2)\omega_{zz} = \omega_0 \sqrt{3/2}$, which coincides with Ref. [2]. Considering a lead levitating particle, $\varrho = 1.09 \times 10^4 \text{ kg/m}^3$, in an AHC of $\mu_0 H_0/R \simeq 75 \text{ T/m}$ [10], we obtain $\omega_0 \simeq 640 \text{ rad s}^{-1} \simeq 2\pi \times 100 \text{ Hz}$.

C. Comparison with cylinders and cuboids

Up to now, we have considered the levitated superconductor with an ellipsoidal shape. It is clear that this is an excellent case for extracting analytical expressions and it represents a pretty good approximation for other shapes. However, the fabrication of such samples is more complicated than other “simpler” shapes such as cylinders or rectangular cuboids. In this section we present numerical results of trapping frequencies, comparing them with the results analytically obtained for ellipsoids.

To compare the different geometries, we consider spheroids with $a = b$, and compare them with cylinders of radius a and length $2c$ and rectangular cuboids with a square cross section of sides $2a$ and length $2c$. Note that the volume of the three samples is not the same: $V_{\text{ell}} = 4\pi a^2 c/3$, $V_{\text{cyl}} = 2\pi a^2 c$, and $V_{\text{cub}} = 8a^2 c$ for the ellipsoid, cylinder, and cuboid, respectively. The mass density ϱ is considered the same. To compare different aspect ratios, we have fixed the value of a and varied the value of c . In all the cases, we have considered that all the samples are in the region where the approximation of the quadrupolar external field holds.

In Fig. 5 we show the calculated frequency for the three shapes as a function of the aspect ratio. It is important to note that, as we shall see in Sec. III D, the equilibrium angle β_0 with respect to rotation varies when c/a changes. In Fig. 5 we show the calculated translational frequencies considering $\beta = \beta_0$ (shown in Fig. 5 for cylinders, cuboids, and ellipsoids). We have also calculated some values for the spheroid to double-check the previous equations and to ensure that the numerical imprecision of the calculations does not affect our results (see Appendix B for further details). The values for cylinders have also been double-checked with Ref. [18].

The main facts we observe are as follows: (i) the equilibrium angle for stability, β_0 , is different depending on the sample and its aspect ratio c/a ; (ii) the evaluated vertical frequencies are larger than the horizontal ones for all the considered geometries; (iii) there is a sudden change in β_0 for the ellipsoids when $c/a = 1$ yielding a kink in the ellipsoid's plot; (iv) for oblate ellipsoids ($c/a < 1$), $\omega_{xx} = \omega_{yy}$ because $\beta_0 = 0$; for prolate ellipsoids ($c/a > 1$), $\omega_{xx} \neq \omega_{yy}$

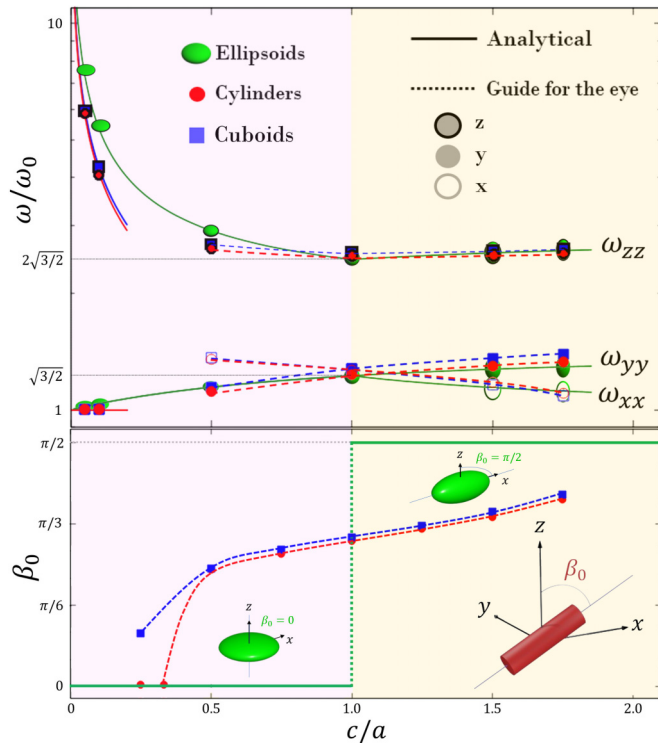


FIG. 5. On top, there are the normalized translational frequencies' components (in logarithmic scale) as a function of c/a for ellipsoids (green ellipsoids), cylinders (red circles), and rectangular cuboids (blue squares). Each point is evaluated from the corresponding stable-rotation angle β_0 . For the same aspect ratio, this stabilization angle is different depending on the geometry. On the bottom, we plot the numerically evaluated stabilization angle as a function of the aspect ratio. Therefore, all frequencies are evaluated with $\beta = \beta_0$ (the corresponding rotational-stability angle) and $\chi = -1$. The lines for the ellipsoids correspond to the analytical expressions [see Eqs. (17)–(19)]. For the cylinders and cuboids, the dotted lines are guides for the eye, and the solid lines are the analytical expression for the small c/a limits [Eqs. (21) and (22)]. The purple region corresponds to oblate ellipsoids and the orange one to prolate ellipsoids. All the dots are numerically calculated values using finite-element methods. The three insets below are schemes of the definition of β_0 using a cylinder as an example (red) and the two β_0 values for oblate and prolate spheroids (green).

because $\beta_0 = \pi/2$; (v) the vertical and horizontal frequencies for cylinders and cuboids are very similar in this comparison; (vi) the frequencies become greater as a greater fraction of the superconducting volume is located closer to the $z = 0$ plane and/or the z axis (suggesting a z -revolution astroid-like shape [19] for the levitated particle).

It is interesting to study the $c \ll a$ limit (very thin samples). It is known that the external susceptibility at small applied fields is $\chi_0 = f_0 a/c$ with $f_0 = 4/(3\pi)$ for cylinders [20] and $f_0 = 0.9094$ (numerically found value) for rectangular cuboids [21]. The resulting vertical and horizontal frequencies are

$$\omega_{zz} = 2\omega_0 \sqrt{f_0 \frac{a}{c}}, \quad (21)$$

$$\omega_{xx} = \omega_{yy} = \omega_0. \quad (22)$$

Note that, in this limit, $\beta_0 = 0$ and ω_{xx} and ω_{yy} are the same for both samples. For thin oblate spheroids, one can also find that $\omega_{zz} \propto \sqrt{a/c}$ and $\omega_{xx} (= \omega_{yy})$ tends to ω_0 .

D. Torques after rotations

Even if the center-of-mass of the ellipsoid is not displaced from the origin of coordinates, the spheroid can rotate. Rotation of microscale diamagnets can exhibit interesting quantum phenomena [22]. In general, the torque on a given magnetized body due to an external field is given by

$$\mathbf{T} = \mu_0 \int_V \mathbf{r} \times (\mathbf{M} \cdot \nabla) \mathbf{H}_a dV. \quad (23)$$

When the spheroid is not rotated (their principal axes point along the coordinates axes) the total torque is zero, although the sample is magnetized. To simplify the treatment of librations we consider that the rotation is over the y axis, represented by the angle β . We can define the librational frequency of the trap as

$$\omega_\beta = \sqrt{\frac{1}{I_y} \left(- \frac{\partial T_y}{\partial \beta} \Big|_{\beta \rightarrow \beta_0} \right)}, \quad (24)$$

where I_y is the moment of inertia of the spheroid with respect to the y axis, $I = (1/5)m(a^2 + c^2) = (4/15)\pi a^2 c(a^2 + c^2)\rho$ for a solid spheroid.

β_0 is the angle with respect to the z axis at which the total torque cancels when only libration is considered. Thus, it represents the rotational equilibrium angle. Ellipsoids, cylinders, and cuboids with identical c/a ratios will stabilize libration at different β_0 angles (see Fig. 5). For rectangular cuboids, there would also be an α or γ dependency, which has not been considered here.

In Ref. [23], the angular frequency was expressed as $\omega_\beta = \frac{c}{a\sqrt{(a/c)^2 + 1}} \sqrt{\frac{15}{4\pi\epsilon} k_\beta}$, where $k_\beta = -\frac{1}{c^2} \frac{\partial T_y}{\partial \beta} \Big|_{\beta \rightarrow 0}$. The term k_β was defined as the effective spring constant of an effective librational oscillator of length c . This definition is similar to ours, although adapted to the vibration of a cantilever.

Although the external field is known, after rotation, we cannot separate the external field in a non-torque-producing term plus a nonzero uniform term [as we did in Eq. (14)]. In the case of a superconducting spheroid with $\chi = -1$, the reaction of the superconductor is the induction of surface currents \mathbf{K} whose value is evaluated from the discontinuity of the tangential component of the \mathbf{B} field at the (rotated) surface of the ellipsoid. In this case, the total torque can also be expressed as

$$\mathbf{T} = \mu_0 \int_S \mathbf{r} \times (\mathbf{K} \times \mathbf{H}_a) dS. \quad (25)$$

We could not find in this case an easy analytical expression for the currents. Approximately, they could be evaluated from the currents at the surface of a sphere [24] adequately distorted to account for the spheroidal shape and then evaluate the above integral. In any case, the expressions would not be simple enough as they are in terms of elliptical integrals. We present in Fig. 6 the librational frequencies evaluated with Eq. (24), after numerically evaluating the torques. The kink

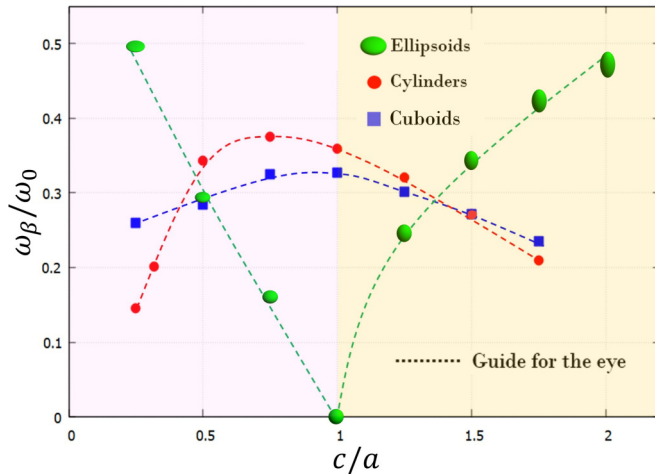


FIG. 6. Librational frequencies for angular vibration of ellipsoids (green), cylinders (red), and rectangular cuboids (blue), as a function of the aspect ratio c/a . Each point is evaluated from the corresponding stable-rotation angle β_0 ; see Fig. 5. The purple region corresponds to oblate ellipsoids and the orange one to prolate ellipsoids. Dashed lines are guides for the eye.

in the librational frequency for the ellipsoids is explained by the change in β_0 from 0 to $\pi/2$ when the ellipsoid passes from oblate to prolate, as shown in Fig. 5.

We observe in Fig. 6 that when c/a is close to unity, cylinders and cuboids are more rigid than spheroids, concerning libration (as expected, since for $c/a = 1$ the ellipsoid is a sphere which can rotate freely, because of the symmetry). However, as the ellipsoid becomes more prolate or more oblate, it becomes more rigidly levitated.

Finally, note that an already rotated ellipsoid, if moved laterally or vertically, would experience, apart from the evaluated restoring force and torque, extra forces that go in the direction perpendicular to the displacement, and, as a consequence, also torques in other directions [see Fig. 2 and Eq. (7)]. The general movement, taking into account all the possibilities, is beyond the scope of this work, but we would like to note that many different possible modes of vibration can appear and that the particular geometry of the levitating sample can play a significant role in their trapping frequencies.

E. Further discussion

The introduced scheme for force and torque evaluation has been presented for the particular case of an AHC trap and a particle that remains in the linear region of the trap. For other types of harmonic traps, the general equations can also be applied, as long as the linear region of the applied field is large enough to keep the ellipsoid inside this region, including its translational and rotational motion.

The ellipsoid geometry (and in general, any geometry beyond the sphere) can follow the symmetry of the traps. That is, one could design a trap that takes advantage of the ellipsoidal symmetry of the levitating particle. In our case, we have a sharp change in the β_0 equilibrium angle, but other types of traps could result in a more tunable behavior. Beyond

ellipsoids, one could fine-tune the geometry of the levitated object to maximize its trap frequencies.

In our work, we neglected the effects of gravity and assumed that, at the particle's equilibrium position, the magnetic force on the particle is zero. Gravity causes the equilibrium position to be shifted, to the point where the magnetic force on the particle cancels the particle's weight. If the z axis is along the vertical direction, the displacement due to gravity is $\Delta z \sim g/\omega_z^2$ (g is the gravity constant). At this displaced position the particle has a magnetic dipole moment, which can affect its rotational properties. It is reasonable to neglect the effects of gravity if the displacement due to gravity Δz is much less than the particle size.

IV. CONCLUSIONS

We have found the external susceptibility matrix, S , that directly relates the magnetization of the ellipsoid with the *uniform applied* field, for all possible relative orientations between them. The key result is that we can express the applied field in the convenient coordinates needed for describing the magnetic system and the magnetization is found directly as a function of the demagnetizing factors, which are tabulated assuming that the field is along one of the principal axes of the ellipsoid.

We have used this result to evaluate the forces received considering a $\chi = -1$ spheroid located at the central region of an anti-Helmholtz coil system. From these forces, the translational (analytically and numerically) and the librational (numerically) trapping frequencies have been evaluated.

The results found, although derived in an idealized case, could be useful in the field of magnetomechanics, since the knowledge of analytical (despite approximate) equations can guide the design of the experimental systems. Moreover, the detailed description of the levitation system and the geometry effects can also serve to calibrate a given experiment and, thus, increase the performance of the experimental setup.

In a more general scope, the described external susceptibility and its consequences could help in performing demagnetization corrections in a broad type of experiments since we have found the external susceptibility tensor as the relation between the internal magnetization (a measure of the reaction of the material) and the *external* applied field (an easily controllable magnitude).

ACKNOWLEDGMENTS

We would like to thank Joachim Hofer and Benjamin A. Stickler for their helpful discussions. We acknowledge financial support from (a) the Spanish Ministry of Science and Innovation MCIN/AEI through Grant No. PID2019-104670GB-I00 and (b) the Horizon Europe 2021-2027 Framework Programme (European Union) through the SUPERMEQ project (Grant Agreement No. 101080143). J.C.-S. acknowledges funding from AGAUR-FI Joan Oró grants (Grant No. 2024 FI-2 00143), Generalitat de Catalunya. W.W. acknowledges funding in part by the Knut and Alice Wallenberg Foundation through a Wallenberg Academy Fellowship, the QuantERA project CMON-QSENS!, and the European Research Council under Grant No. 101087847 (ERC CoG

SuperQLev). G.H. acknowledges support from the Swedish Research Council (Grant No. 2020-00381). C.N. acknowledges support as a Serra Hünter Fellow. This research was funded in whole or in part by the Austrian Science Fund (FWF) (10.55776/esp525).

APPENDIX A: DETAILS OF THE LINEAR APPROXIMATION

In this Appendix, we will explicitly derive Eq. (15) when considering an ellipsoid centered at the point \mathbf{r}_0 and located in the linear region of the AHC field. Since the field is linear, $\mathbf{H}_a(\mathbf{r}) = \mathbb{G}\mathbf{r}$, where \mathbf{r} is the position vector and \mathbb{G} is a 3×3 field gradient matrix, $\mathbb{G}_{ij} = \partial H_{a,i} / \partial x_j$ [where $i, j = 1, 2, 3$ and $(x_1, x_2, x_3) = (x, y, z)$]. In our case, after Eq. (13), $\mathbb{G} = (H_0/R) \text{diag}(-1, -1, 2)$.

Consider an ellipsoid displaced from the origin of the trap such that its center is at \mathbf{r}_0 (Fig. 7, left). Any point of the ellipsoid is subjected to an external field given by $\mathbf{H}_a(\mathbf{r}) = \mathbb{G} \cdot (\mathbf{r}_0 + \mathbf{r}') = \mathbb{G}\mathbf{r}_0 + \mathbb{G}\mathbf{r}' = \mathbf{H}_a(\mathbf{r}_0) + \mathbf{H}_a(\mathbf{r}')$, where $\mathbf{r}' = \mathbf{r} - \mathbf{r}_0$. Consequently, the applied field at any point of the ellipsoid is a uniform field (the field at the center of the ellipsoid) plus a quadrupolar field with origin at the center of the ellipsoid.

The force over the ellipsoid can be evaluated from

$$\mathbf{F} = \mu_0 \int_V [\mathbf{M}(\mathbf{r}) \cdot \nabla] \mathbf{H}_a(\mathbf{r}) d^3\mathbf{r}. \quad (\text{A1})$$

Taking into account that our \mathbb{G} is a constant and diagonal matrix (i.e., it does not depend on position), the above expression can be rewritten as

$$\mathbf{F} = \mu_0 \int_V \mathbb{G}\mathbf{M}(\mathbf{r}) d^3\mathbf{r}. \quad (\text{A2})$$

Now, as the ellipsoid's material is assumed linear, we can write $\mathbf{M}(\mathbf{H}_a(\mathbf{r})) = \mathbf{M}(\mathbf{H}_a(\mathbf{r}_0)) + \mathbf{M}(\mathbf{H}_a(\mathbf{r}')) \equiv \mathbf{M}_1 + \mathbf{M}_2(\mathbf{r}')$. Note that $\mathbf{H}_a(\mathbf{r}_0)$ acts as a uniform field at every point of the ellipsoid, so \mathbf{M}_1 is also uniform for ellipsoids (see Fig. 7, middle) and can be evaluated from Eq. (5). \mathbf{M}_2 depends on the position inside the ellipsoid, but it has the symmetry of a

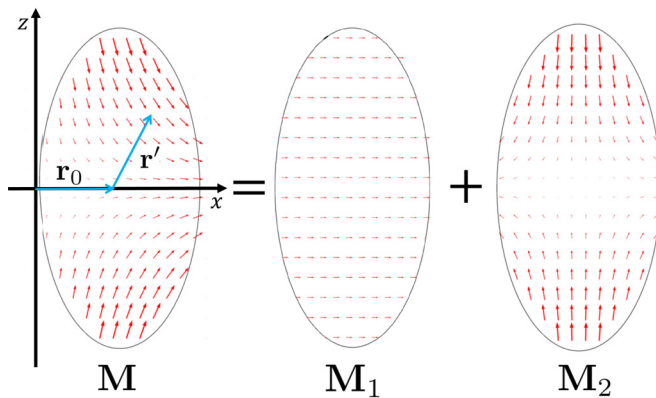


FIG. 7. The total magnetization of a spheroid displaced along the x axis \mathbf{M} (left, red arrows) can be expressed as the superposition of the magnetization \mathbf{M}_1 due to a uniform field equal to that at the center of the spheroid (center, red arrows), plus the magnetization \mathbf{M}_2 induced by the currents generated by the quadrupolar field at the center of the trap (right, red arrows).

quadrupolar field (see Fig. 7, right). The above equation becomes

$$\mathbf{F} = \mu_0 \int_V \mathbb{G}\mathbf{M}_1 d^3\mathbf{r} + \mu_0 \int_V \mathbb{G}\mathbf{M}_2(\mathbf{r}') d^3\mathbf{r}'. \quad (\text{A3})$$

Since \mathbb{G} does not depend on position and \mathbf{M}_1 is a uniform vector field, we get

$$\mathbf{F} = \mu_0 V \mathbb{G}\mathbf{M}_1 + \mu_0 \mathbb{G} \int_V \mathbf{M}_2(\mathbf{r}') d^3\mathbf{r}'. \quad (\text{A4})$$

Because of the symmetry of $\mathbf{M}_2(\mathbf{r}')$ (see Fig. 7, right), the remaining integral must be zero. Rewriting back the \mathbb{G} matrix in terms of derivatives, and using $\mathbf{M}_1 = \mathbb{S}\mathbf{H}_a(\mathbf{r}_0)$ [Eq. (5)], we obtain Eq. (15) of the main text:

$$\mathbf{F} = \mu_0 V \mathbb{G}\mathbf{M}_1 = \mu_0 V (\mathbb{S}\mathbf{H}_a \cdot \nabla) \mathbf{H}_a \Big|_{\mathbf{r}=\mathbf{r}_0}. \quad (\text{A5})$$

Note that the field and the derivatives should be evaluated at $\mathbf{r} = \mathbf{r}_0$.

Observe that this argument of considering only the external field at the center of the ellipsoid does not hold when treating rotational modes, since, in this case, the rotation could produce a net angular momentum. For torque evaluation, a numerical calculation of the Maxwell stress tensor inside the ellipsoid is performed (see Sec. III D and Appendix B). Note also that we have not imposed any geometric condition for the levitating particle (apart from symmetry). Therefore, the argument applies to ellipsoids, as well as to cylinders and prisms, with the significant difference that the magnetization generated by the uniform field $\mathbf{H}_a(\mathbf{r}_0)$ would not remain uniform in these last two shapes.

APPENDIX B: NUMERICAL CALCULATIONS

The numerical calculations were performed using finite-element method simulation using COMSOL Multiphysics software. The Magnetic Fields (mf) interface was used employing the A formulation to calculate the magnetic vector potential \mathbf{A} of a magnetic system.

The simulation space was set as a sphere with a radius $D \gg a, b,$ and c ($D \simeq 20a$), with the levitating particle at the center. The boundary conditions were set to have a quadrupolar field, Eq. (13), at the surface of the large sphere. In this way, we ensure that the ellipsoid is situated in a quadrupolar field and does not disturb the field at greater distances. As the system behaves linearly (concerning both the material permeabilities and the external field), the particle's absolute length dimensions are irrelevant for numerical calculations; only its relation to the entire simulated space has to be taken into account.

The superconducting levitated particle (modeled as an ellipsoid, a cylinder, or a rectangular cuboid) was simulated as a linear material with zero magnetic permeability. In practice, the relative permeability of the material for the simulation was set to 10^{-4} , which gives a good approximation to a zero-magnetic-permeability material. The rest of the space was simulated as a vacuum with a relative magnetic permeability equal to 1.

The Maxwell stress tensor was evaluated to determine the total net force and torque exerted on each particle. The equilibrium angle β_0 for each particle was calculated by measuring

the torque for different angles. A linear interpolation of angle against torque was performed, and the β_0 angle was taken as the abscissa intercept of the plot.

To calculate the different displacement frequencies ω_{xx} , ω_{yy} , and ω_{zz} for all geometries, five force calculations were performed at different positions for each of the three spatial coordinates. Specifically, five force calculations were done with different x positions while keeping $z = y = 0$,

and similarly for y and z . For all cases, we used the corresponding β_0 for each particle. The slope of the force against the position plot was then used to calculate the frequency of the levitating particle along the three spatial dimensions.

Finally, the torque for five different angles centered at β_0 was calculated and the librational frequencies were obtained from the slope of that torque against the displaced angle.

-
- [1] D.-X. Chen, J. A. Brug, and R. B. Goldfarb, Demagnetizing factors for cylinders, *IEEE Trans. Magn.* **27**, 3601 (1991).
- [2] O. Romero-Isart, L. Clemente, C. Navau, A. Sanchez, and J. I. Cirac, Quantum magnetomechanics with levitating superconducting microspheres, *Phys. Rev. Lett.* **109**, 147205 (2012).
- [3] M. Cirio, G. K. Brennen, and J. Twamley, Quantum magnetomechanics: Ultrahigh- q -levitated mechanical oscillators, *Phys. Rev. Lett.* **109**, 147206 (2012).
- [4] M. Gutierrez Latorre, G. Higgins, A. Paradkar, T. Bauch, and W. Wieczorek, Superconducting microsphere magnetically levitated in an anharmonic potential with integrated magnetic readout, *Phys. Rev. Appl.* **19**, 054047 (2023).
- [5] C. Timberlake, G. Gasbarri, A. Vinante, A. Setter, and H. Ulbricht, Acceleration sensing with magnetically levitated oscillators above a superconductor, *Appl. Phys. Lett.* **115**, 224101 (2019).
- [6] J. Prat-Camps, C. Teo, C. C. Rusconi, W. Wieczorek, and O. Romero-Isart, Ultrasensitive inertial and force sensors with diamagnetically levitated magnets, *Phys. Rev. Appl.* **8**, 034002 (2017).
- [7] A. Vinante, P. Falferi, G. Gasbarri, A. Setter, C. Timberlake, and H. Ulbricht, Ultralow mechanical damping with Meissner-levitated ferromagnetic microparticles, *Phys. Rev. Appl.* **13**, 064027 (2020).
- [8] B. R. Slezak, C. W. Lewandowski, J.-F. Hsu, and B. D'Urso, Cooling the motion of a silica microsphere in a magneto-gravitational trap in ultra-high vacuum, *New J. Phys.* **20**, 063028 (2018).
- [9] M. G. Latorre, J. Hofer, M. Rudolph, and W. Wieczorek, Chip-based superconducting traps for levitation of micrometer-sized particles in the meissner state, *Supercond. Sci. Technol.* **33**, 105002 (2020).
- [10] J. Hofer, R. Gross, G. Higgins, H. Huebl, O. F. Kieler, R. Kleiner, D. Koelle, P. Schmidt, J. A. Slater, M. Trupke, K. Uhl, T. Weimann, W. Wieczorek, and M. Aspelmeyer, High- q magnetic levitation and control of superconducting microspheres at millikelvin temperatures, *Phys. Rev. Lett.* **131**, 043603 (2023).
- [11] M. G. Latorre, A. Paradkar, D. Hambreus, G. Higgins, and W. Wieczorek, A chip-based superconducting magnetic trap for levitating superconducting microparticles, *IEEE Trans. Appl. Supercond.* **32**, 1800305 (2022).
- [12] J. A. Zielińska, F. van der Laan, A. Norrman, M. Rimplinger, R. Reimann, L. Novotny, and M. Frimmer, Controlling optomechanical libration with the degree of polarization, *Phys. Rev. Lett.* **130**, 203603 (2023).
- [13] C. Navau, S. Minniberger, M. Trupke, and A. Sanchez, Levitation of superconducting microrings for quantum magnetomechanics, *Phys. Rev. B* **103**, 174436 (2021).
- [14] This rotation representation was used because, in most of the paper, we will consider $a = b$, and rotation over z will not affect anything and only the angle β will be relevant.
- [15] E. C. Stoner, XCVII. demagnetizing factors for ellipsoids, *Lond. Edinb. Dublin Philos. Mag. J. Sci.* **36**, 803 (1945).
- [16] D. Takahashi and V. C. Oliveira, Jr., Ellipsoids (v1.0): 3-D magnetic modelling of ellipsoidal bodies, *Geosci. Model Dev.* **10**, 3591 (2017).
- [17] M. Beleggia, M. D. Graef, and Y. Millev, Demagnetization factors of the general ellipsoid: An alternative to the Maxwell approach, *Philos. Mag.* **86**, 2451 (2006).
- [18] J. Hofer, A numerical approach to levitated superconductors and its application to a superconducting cylinder in a quadrupole field, *Phys. Scr.* **99**, 095526 (2024).
- [19] J. D. Lawrence, *A Catalog of Special Plane Curves* (Dover Publications, New York, 1972), p. 218.
- [20] J. R. Clem and A. Sanchez, Hysteretic ac losses and susceptibility of thin superconducting disks, *Phys. Rev. B* **50**, 9355 (1994).
- [21] D.-X. Chen, C. Navau, N. Del-Valle, and A. Sanchez, Perpendicular critical-state susceptibility of square superconducting films, *Appl. Phys. Lett.* **92**, 202503 (2008).
- [22] B. A. Stickler, K. Hornberger, and M. S. Kim, Quantum rotations of nanoparticles, *Nat. Rev. Phys.* **3**, 589 (2021).
- [23] A. Kamra, M. Schreier, H. Huebl, and S. T. B. Goennenwein, Theoretical model for torque differential magnetometry of single-domain magnets, *Phys. Rev. B* **89**, 184406 (2014).
- [24] J. Hofer and M. Aspelmeyer, Analytic solutions to the Maxwell-London equations and levitation force for a superconducting sphere in a quadrupole field, *Phys. Scr.* **94**, 125508 (2019).